Optical constants of hydrogenated amorphous carbon in the range 0–100 eV

G. Curro', F. Neri, and G. Mondio
Istituto di Struttura della Materia, Universita' di Messina, Salita Sperone 31, 98166 Sant'Agata, Messina, Italy

G. Compagnini
Istituto di Metodologie e Tecnologie per la Microelettronica, Consiglio Nazionale delle Ricerche, Corso Italia 57, 95129 Catania, Italy

G. Foti
Dipartimento di Fisica, Universita'di Catania, Corso Italia 57, 95129 Catania, Italy
(Received 15 July 1993; revised manuscript received 12 November 1993)

The dielectric behavior of hydrogenated amorphous carbon samples, prepared by keV-Ar-ion bombardment of a polystyrene matrix, in the energy range 0–100 eV has been studied in connection with the change in hydrogen content. The wide-ranging results obtained by means of electron-energy-loss spectroscopy in reflection mode have been successfully compared with the optical constants available in the 1–6 eV range, resulting from the combined use of transmittance and reflectance experimental spectra. A strong rearrangement of the $\sigma \rightarrow \sigma^*$ transitions is evidenced in the bulk loss function $\mathrm{Im}(-1/\tilde{\epsilon})$ together with a change in the relative oscillator strengths, on going from pure amorphous carbon to the most hydrogenated ($x_H = 40\%$) α-C:H sample.

I. INTRODUCTION

The recently growing interest in amorphous carbon α-C and hydrogenated amorphous carbon α-C:H films lies in their unusual properties such as inertness against bases and acids, hardness, optical transparency in the infrared range, high refractive index, and chemical passivation capabilities.[1–3] The possibility of changing the physical and chemical characteristics of these materials by adopting different preparation and thermal treatment methods opened the way to much technologically aimed research.

So far, the process largely adopted to prepare α-C films has been sputtering by heavy ions of inert species or evaporation from natural carbon sources, whilst α-C:H films have been prepared almost exclusively by plasma deposition of hydrocarbons,[4] such as ethylene, or by sputtering of graphite in a hydrogen atmosphere.[5] However, ion bombardment of graphite appears to be the most suited technique to produce α-C, because in this way it is easy to control the degree of amorphization of the sample, and then its resulting structural and electronic properties, by just adjusting the ion-beam parameters in the desired way. Recently, this approach has been developed also to prepare α-C:H films: controlled fluences of keV ions are accelerated onto a hydrocarbon polymeric matrix (e.g., polystyrene), and the energy release which follows inside the matrix causes the creation of different kinds and amounts of defects (and eventually complete amorphization), thus modifying the hydrogen content and possibly creating a graphitic-cluster size distribution much more accurately than with the above-mentioned techniques. Thus, by just tuning the ion-beam parameters (flux and energy) and possibly by thermal conditioning treatment, it is possible to obtain an enormous variety of different materials.

It has been realized that this extraordinarily vast family of materials originates from the unique possibility for carbon to form two bonding-coordination structures in various relative amounts intermixed in the same specimen, namely planar sp^2 and tetrahedral sp^3 configurations. This has suggested that attempts to analyze the local structure and to deduce the ratio of sp^2 to sp^3 contributions can provide some further understanding of these materials.

Whilst it is relatively easy to monitor the strong change in the properties of hydrogenated amorphous carbon films, to analyze their origin from a theoretical viewpoint has been shown to be a hard task, due to difficulties which arise in trying to state the potentials occurring in the amorphous site distribution. An attempt has been made by Robertson and O'Reilly[7] whose calculations suggested that the behavior of these films is connected to the hydrogen concentration and to the sp^2-to-sp^3 ratio; they pointed out that ion bombardment affects the medium-range order parameters (in the 5–30-Å range), inducing graphitic clustering whilst reducing the hydrogen fraction. In that way, quantities such as the optical gap could be analytically related to the medium-sized clusters of trigonal character. It is worth remembering also that amorphization of the original polymers has an effect, in the sense that the resulting structure is not microcrystalline (as it is, for instance, in glassy carbon), but can be viewed as the effect of a strong-bond rearrangement leading to graphitic islands, each formed by a statistically distributed number of five-, six-, and sevenfold benzoid rings, linked to one another by tetrahedral σ bonds involving hydrogen atoms.

Concerning α-C, a theoretical analysis based on *ab initio* dynamical calculations has shown that the more stable configuration is when 85% sp^2 character is present.[8] From the experimental point of view, much work has been done, aiming to better characterize both structural and electronic properties of these materials. However, almost all these measurements were carried out on plasma-

deposited samples from polymeric hydrocarbons, e.g., benzene, or on films prepared by sputtering a carbon electrode in hydrogen atmosphere. Near-infrared–visible–uv normal absorption measurements[9] carried out on α-C:H films deposited by sputtering a carbon cathode in $Ar+H_2$ atmosphere (30% hydrogen content in the resulting film) have shown that these samples, as well as α-C evaporated films, have semiconductor character with relatively large π density of states close to the Fermi level. In the same paper, electron-spin resonance measurements are reported showing that the conductivity of those materials is raised by the presence of localized gap states due to the five- and sevenfold carbon rings, but these states do not affect the absorption coefficient.

For plasma-deposited films, Fink *et al.*[10] performed electron-energy-loss spectroscopy (EELS) on 1000-Å-thick α-C:H films with various H concentrations and at various annealing temperatures. Their extended x-ray-absorption fine-structure analysis evidenced the amorphous and not microcrystalline structure of the samples, while the near-edge spectral profile x-ray-absorption near-edge structure suggested a strong π contribution to the bonding. In Ref. 11 are reported further EELS analysis in the 0–40-eV energy-loss range and the determination of the complex dielectric function via a Kramers-Kronig transform procedure; by using a well-known sum rule, the authors found the sp^2-to-sp^3 ratio to be $\frac{2}{3}$ for all the samples, disregarding the hydrogen content.

On the other hand, not much experimental work has been carried out on amorphous carbon prepared by keV-ion bombardment of hydrocarbon polymers in order to characterize their electronic and optical properties, so far. Terrasi *et al.*[12] performed a synchrotron-radiation ultraviolet-photoemission-spectroscopy investigation on polystyrene samples bombarded with 0.5-keV Ar^+ ions at different ion fluences (ranging from 10^{14} cm^{-2} to 10^{15} cm^{-2}), concluding that the ion damage causes the valence-band spectrum to evolve from that typical of a molecular solid to that of amorphous carbon or very damaged highly oriented pyrolytic graphite (HOPG).

We have carried out an optical (reflectance and transmittance) and electronic analysis on two differently dosed α-C:H and one α-C films, the latter having been produced by irradiating a HOPG sample with a high enough Ar-ion flux. The aim of this work has been to determine the dielectric functions of these materials in an energy range as large as 100 eV, and to establish a trend in the optical behavior just by following the evolution of single-particle valence-band scattering and plasmonic structures present in the loss function $\mathrm{Im}(-1/\tilde{\epsilon})$. It is worth remembering that the interpretation of the data must take into account the origin and treatment of the pristine polystyrene samples as well as the final hydrogen content and the ion-beam parameters. No particular account is taken of the α-C preparation, since the high ion flux used ensures a saturated amorphization spread throughout a large enough part of the sample.

The paper is organized in four main parts. In Sec. II a sketch of the experimental setup and sample preparation is reported; Sec. III contains a description of the procedure used to get the optical constants from the reflectance and transmittance spectra, while Sec. IV shows the deconvolution procedure used to get the dielectric function in the extended energy range through the use of EELS data; in Sec. V the experimental findings are reported and discussed.

II. SAMPLE PREPARATION AND EXPERIMENTAL SETUP

The original polystyrene films with average thickness of 300 nm were deposited on a fused silica or silicon substrate by centrifuging a solution of $CHCl_3$. Pristine hydrogenated amorphous carbon (HAC) films were then prepared by sweeping a 1×1-in^2 polystyrene area with a 200-keV C^+-ion beam for 500 sec at 100-nA beam current. The resulting layers were quite transparent, with an optical gap of 2.0 eV and 45% hydrogen concentration. After that, the pristine HAC samples were irradiated with 300-keV Ar^+ ions at fluences of 5×10^{14} and 10^{16} ions/cm^2, allowing for an ion range larger than the sample thickness in order to get uniform damage. The α-C was prepared by Ar-ion bombardment of a HOPG surface with a high enough ion current and 2.0-keV beam energy until a complete amorphization was obtained. A microgranular polycrystalline graphite sample was used as a reference to get the sp^2 site percentages for all the materials concerned.

Hydrogen concentrations were measured by the elastic-recoil technique[13] with 2.0-MeV He atoms as the primary beam: this allowed us to get a depth resolution of 40 nm and a sensitivity up to 1% hydrogen concentration (bound plus unbound H). A measurement of the film thickness (with a Talystep) together with detection of the amount of carbon atoms (through proton backscattering) and of the hydrogen outgassing (through quadrupole mass spectroscopy) allowed the determination of the mass density of the films, as discussed in detail in Ref. 14. The optically derived complex dielectric constants as well as the optical energy gaps of the samples were obtained by performing uv-visible spectrophotometry, namely transmittance and reflectance measurements in the wavelength range 200–1100 nm, with a Lambda 2 Perkin-Elmer double-beam spectrometer. The amorphous carbon film was obtained by bombarding a HOPG sample with a high-fluence Ar^+-ion beam at keV energy. The energy gaps and the hydrogen concentrations are summarized in Table. I.

The electron-energy-loss measurements were performed in a VG-Instrument ultrahigh-vacuum chamber at a base pressure in the low 10^{-9} Torr. Oxygen-free samples were obtained *in situ* by bombarding the surfaces

TABLE I. Hydrogen contents x_H, mass densities, and energy gaps of the materials of interest.

Sample, x_H (%)	ρ (g/cm^3)	E_g (eV)
0	2.2	0.2
15	1.6	0.5
40	1.1	1.5

with low-current slow Ar^+ ions (2.0-keV beam energy) for a cycle time as short as about 10 min, and checking the oxygen content by the Auger technique. This cleaning procedure is believed not to modify the nominal structural properties of the sample, provided that low (time-integrated) ion fluxes and low beam energies are adopted. Obviously, the α-C sample is totally unaffected by the sputtering procedure, due to its preparation characteristics.

Reflection electron-energy-loss spectroscopy (REELS) measurements were performed at 2.0-keV primary-electron energy, at an incidence angle of about 40°; the ejected-electron analyzer was a VG-CLAM 100 used in constant-analyzer-energy mode; the total (analyzer plus electron gun) energy resolution was assumed to be the elastic-peak half width at half maximum (HWHM), and it was found to be nearly 0.35 eV for all the spectra.

III. DETERMINATION OF THE OPTICAL CONSTANTS IN THE LOW-ENERGY RANGE

The reflectance and transmittance measurements allow us to obtain the real ϵ_1 and imaginary ϵ_2 parts of the dielectric function in the range 1–6 eV using a least-squares fit as suggested by Fouruhi and Bloomer.[15] They calculated the transition probabilities from first-order time-dependent perturbation theory, obtaining $\epsilon_2(E)$ as proportional to the number of possible transitions. Assuming a complete lack of momentum conservation and parabolic conduction and valence bands, it is possible to obtain the following expression:

$$k(E)=A(E-E_g)/(E^2-BE+C) ,$$

where A,B,C are constants which satisfy $A,B,C \geq 0$ and $4C-B^2 \geq 0$, and E_g is the energy gap; k is the imaginary part of the refractive index while n (the real part) can be calculated through the Kramers-Kronig relation which yields:

$$n(E)=n_\infty+(B_0E+C_0)/(E^2-BE+C) ,$$

where B_0 and C_0 are functions of A, B, C, and E_g; n_∞ is the high-frequency limit for n.

Experimental spectra and results for several hydrogenated amorphous carbon thin films are reported elsewhere.[16] The resulting dielectric constants for the materials concerned are drawn in Fig. 7 below, together with the same functions obtained through REELS. However, it must be noted that the approximation of parabolic bands, although necessary to obtain a unified description of the whole spectral range with the Fouruhu method, does not take into account the observed exponential tail in the electronic density of states in the region of the forbidden gap. These reasons led several authors to explore the exponential region (often called the Urbach region) with alternative measurements such as photothermal deflection spectroscopy (PDS) to obtain the optical constants.

IV. THE SPECTRAL DECONVOLUTION METHOD

The differential REEL cross section for an electron beam impinging on a sample at non-normal incidence with primary energy E_p and wave vector k_0 can be written as[17]

$$\frac{d^3W}{dE\,d^2\Omega} \sim \tau\,\mathrm{Im}\left[\frac{-1}{\epsilon}\right]\frac{1}{\theta^2+\theta_E^2} + \frac{8}{k_0}\mathrm{Im}\left[\frac{-1}{\epsilon+1}\right]\frac{\theta}{(\theta^2+\theta_E^2)^2}\left[1+\frac{\theta_E\,tg\alpha}{\theta}\right] , \quad (1)$$

where E is the energy loss, α the incidence angle, θ the scattering angle, and $\theta_E=E/2E_p$; the factor τ is an equivalent sample thickness, which represents the effective path length traveled by the electron inside the sample, defined as

$$\tau=\left[\frac{d}{\cos\alpha}\right]\frac{\exp(-2d/\Lambda\cos\alpha)}{1-\exp(-2d/\Lambda\cos\alpha)} ,$$

where d is the spacing between atomic planes and Λ the electron mean free path at the chosen primary energy. This last quantity has been deduced by a universal function successfully used in the case of organic compounds.[18,19] As can be seen in Eq. (1), the cross section is the sum of two contributions, the bulk and the surface contributions.

Starting from this relation, the theoretical bulk and surface yields which build up the REEL spectrum are obtained by simply integrating it over the acceptance solid angle or, which is the same, over the transferred momentum range of limits q_+ and q_-:

$$\theta_+=\left[\frac{q_+^2}{k_0^2}-\theta_E^2\right]^{1/2} , \quad \theta_-=\left[\frac{q_-^2}{k_0^2}-\theta_E^2\right]^{1/2} ,$$

related to the corresponding scattering angles by:

$$q_\pm=\frac{2\pi}{12.25}\{(E_p)^{1/2}\pm(E_p-E)^{1/2}\} .$$

The resulting function, which depends only on τ, E_p, and k_0, has been used to fit the experimental spectra.

The measured total yield in REELS is generally considered as the superposition of various contributions arising from different physical effects which follow the interaction of the electron probe with the solid. Based on this model, the global spectrum can be described as the following sum:

$$Y(E)=P(E)+B(E)+K(E) , \quad (2)$$

where $P(E)$ is the elastic peak, $B(E)$ is the background which includes also the multiple-scattering structures, and $K(E)$ is the loss function. The elastic peak $P(E)$ has been represented by a Gaussian curve. The background $B(E)$ results from a self-consistent calculation pointed out by Tougaard and Kraaer.[20] The model function adopted to describe the loss cross section $K(E)$ is the sum of a number of Drude-type contributions; this func-

tion enters an iterative Kramers-Kronig transform procedure which eventually allows the calculation of the dielectric function in terms of its real and imaginary parts, provided a well-suited normalization[19] is performed in such a way as to match the value of $\tilde{\epsilon}$ at very low energy loss, this last value being deduced from optical reflectivity measurements.

V. RESULTS AND DISCUSSION

In Fig. 1 the experimental REELS data for two α-C:H samples (those with to 40% and 15% hydrogen fractions, respectively) together with the raw spectrum of Ar^+-beam-damaged amorphous carbon are reported; all the spectra are normalized to their respective elastic-peak intensities, which allows a comparison free of possible instrumental effects. The line shapes of the spectra of the hydrogenated samples appear to be very similar to each other, the most relevant difference being in the low-energy-loss range which reflects the change in the electron conductivity in the two materials.

After applying the fitting procedure described in the previous section, the pure surface and bulk single-scattering loss functions are evaluated together with the complex dielectric functions. The former are reported in Figs. 2 and 3; a remarkable shift of the $\pi+\sigma$ plasmon peak is clearly evidenced on varying the sample (specifically, the plasmon energy moves towards lower values on going away from α-C, which corresponds to increasing the hydrogen content), as well as a change in the oscillator strengths in the low-energy-loss region, which shows up mainly in the increase of single-particle excitation structures in the hydrogenated samples with respect to the unhydrogenated one, overwhelming the possible π plasmon. The structureless π band in the α-C measured cross section confirms the high degree of amorphization achieved in that case.

The dielectric constants, extended in an energy-loss range as large as 60 eV, are shown in Fig. 4; strong differences in the dielectric behavior of the various materials are now even more marked both in the real and imaginary part of $\tilde{\epsilon}=\epsilon_1+i\epsilon_2$. In particular, the ϵ_2 curves show a decrease in the ratio between the low-energy-loss (about 0–10-eV) contribution, which is connected to the π-electron transitions, and the remaining high-energy-loss part, mainly of σ character, on increasing the hydro-

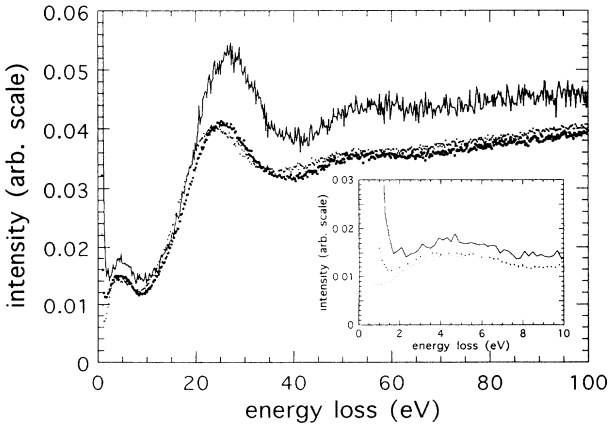

FIG. 1. Raw REEL spectra of the different materials: solid line, α-C; big dots, α-C:H, $x_H=15\%$; small dots, α-C:H, $x_H=40\%$. The inset shows the same curves magnified in the energy region 0–10 eV.

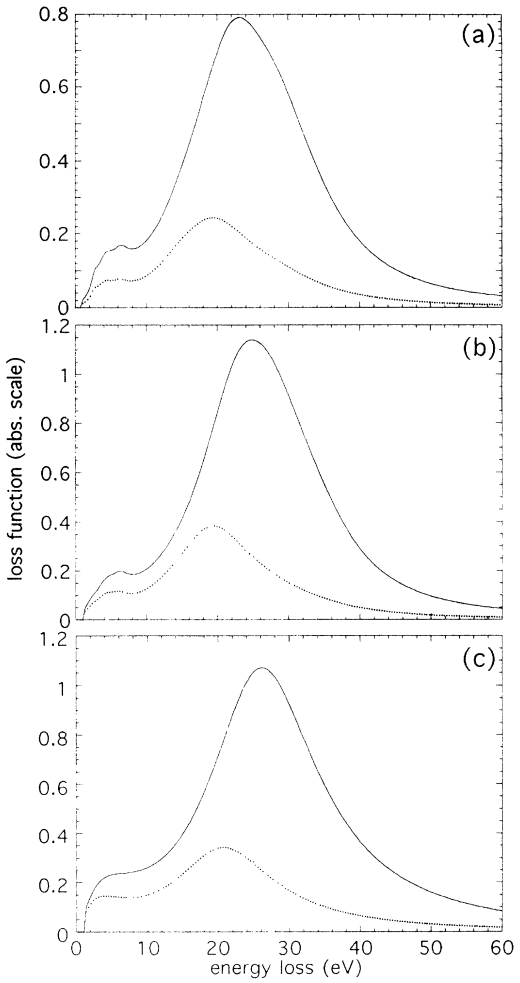

FIG. 2. Surface (dotted line) and bulk (solid line) single-scattering loss functions: (a) α-C:H, $x_H=40\%$; (b) α-C:H, $x_H=15\%$; (c) α-C.

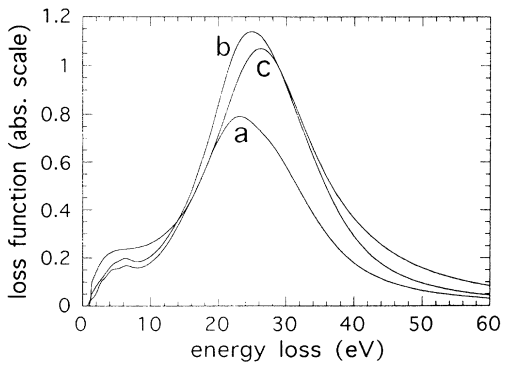

FIG. 3. Comparison of the bulk single-scattering loss functions of the different samples (same labeling as in Fig. 2).

gen fraction. Moreover, a redistribution of intensity among the various absorption structures (at least four of them are positioned in the first 10 eV) is recognizable in the hydrogenated samples.

The difference between the hydrogenated amorphous carbon films and the highly damaged HOPG is strongly evidence in the fact that the latter is characterized by a single absorption peak centered at about 2.5 eV, whose width is about 2 eV (FWHM): this structure is not visible in the α-C:H spectra. Moreover, the remaining part of the π contribution in the unhydrogenated carbon sample shows up as a flat band separated from the σ region by a shallow and large minimum.

Another observation regards the large σ absorption band which moves from 14.5 eV, where it is in the highest-x_H α-C:H, to about 13 eV, characteristic of the lowest-x_H sample. Such bands appear to be as large as the corresponding contribution in the α-C spectrum; this could be interpreted as stemming from the superposition of many different statistically distributed site contributions to the σ-absorption cross section. The analogous structure in α- C is positioned at about 13.5-eV energy loss.

In Figs. 5 and 6 the effective number $n_{\text{eff}}(E)$ of electrons per atom participating in the excitations is reported both for the π-electron contribution only and for the total $(\pi+\sigma)$-electron contribution in the whole energy-loss range probed. The $n_{\text{eff}}(E)$ values come from the use of a well-known sum rule:

$$n_{\text{eff}}=\frac{M}{1300\rho}\frac{1}{s}\int_0^{E_0}E\epsilon_2(E)dE\ , \tag{3}$$

where M is the molecular weight, coming from a simple averaging of the carbon and hydrogen contents, ρ is the mass density in g/cm^3, and s is a static screening factor which takes into account the screening of the π electrons due to the dielectric constant of the remaining σ electrons. The screening factor s is strictly related to the way in which σ electrons locally reorganize following the π-band excitations and can be described, at least phenomenologically, as (see Ref. 21):

$$s=\frac{1}{1+\epsilon_1^{\sigma}(E_{\pi})}\ ,$$

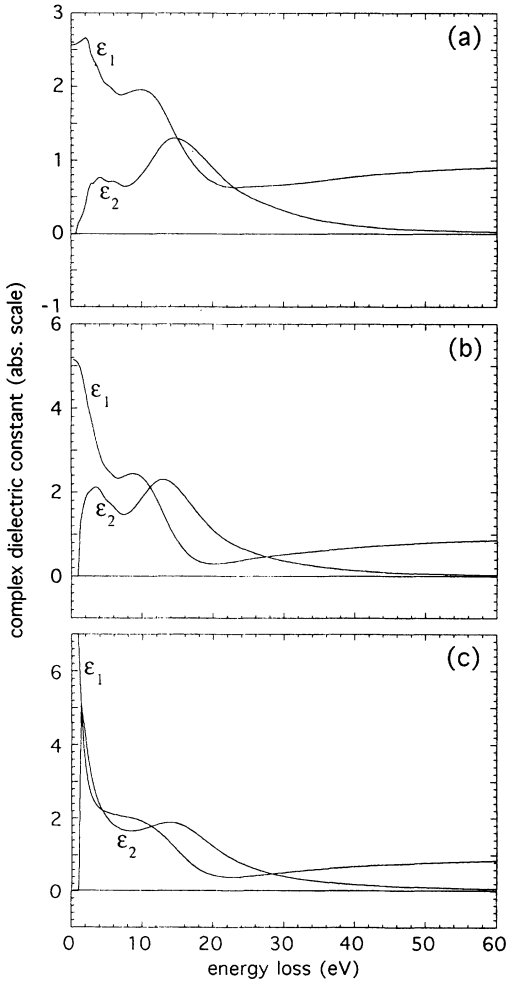

FIG. 4. Real and imaginary parts of the complex dielectric functions $\tilde{\epsilon}(E)$: (a) α-C:H, $x_H=40\%$; (b) α-C:H, $x_H=15\%$; (c) α-C.

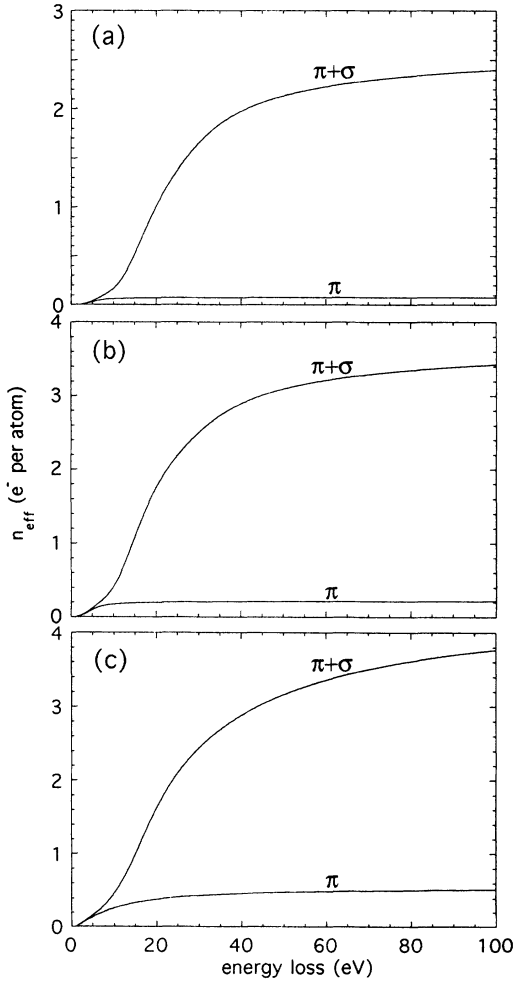

FIG. 5. Effective numbers of electrons per atom participating in the scattering process, $n_{\text{eff}}(E)$, both for the π electrons only and for the total $\pi+\sigma$ electrons. (a) α-C:H, $x_H=40\%$; (b) α-C:H, $x_H=15\%$; (c) α-C.

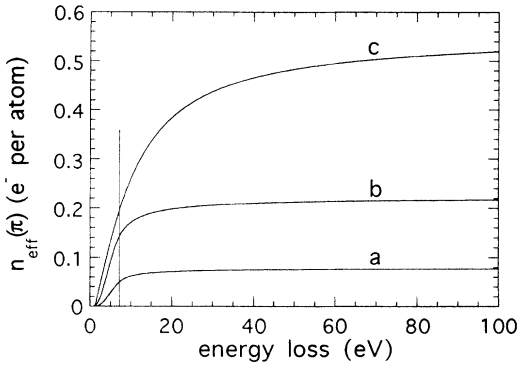

FIG. 6. Comparison of the effective number of π electrons involved in the absorption process (labeling as in Fig. 2); a straight vertical line marks the cutoff energy limit (7 eV).

in which $\epsilon_1^{\sigma}(E_{\pi})$ is the value of the real part of the dielectric function due only to the σ-band transitions, calculated at the observed π-plasmon position. The latter is about 5 eV for all the samples, as it comes from the ϵ_2 curves; the exact value of E_{π} is not needed because of the slow variation of ϵ_1^{σ} in the energy range around 5 eV. The above screening factor has to be interpreted as the effective number of π electrons per valence electron participating in the collective oscillation, after considering the influence of the σ transitions: the bigger the s factor, the smaller is the screening.

By assuming as a cutoff energy for the π-initial-state transitions an energy-loss value $E=7$ eV, we find that s slightly changes on varying the material; its values are reported in Table II together with the percentages of sp^2 sites consequently calculated using Eq. (3) and the measured polycrystalline-graphite value of n_{eff} (7 eV), i.e., 0.40 ($s=0.345$) electrons per atom. Recently it has been suggested[22] that in principle the nonsaturation of n_{eff} due to the π electrons around 7 eV rules out the possibility of obtaining the percentage of sp^2 sites from the complex dielectric constant, since it is not possible to separate the π from the σ contributions to the absorption. However, it has been theoretically and experimentally[21–25] demonstrated that the $\pi \rightarrow \pi^*$ transitions in amorphous carbon (either hydrogenated or not) are exhausted at about 7 eV; moreover, even from the present ϵ_2 curves a separation is clearly visible at about 7–9 eV between π and σ absorption bands. This fact, together with the relatively slowly varying behavior of $n_{\text{eff}}(\pi)$ around the chosen cutoff energy for all the samples, allows us to obtain the sp^2-site percentage from Eq. (3), with acceptable approximation.

The sp^2 percentage for the fully amorphized carbon sample is slightly smaller than that previously reported in the literature,[8] i.e., 85%, with a screening factor very similar to that of pure HOPG. It is worth noting that the sp^2-to-sp^3 ratios we have obtained from the present REELS analysis are similar to those previously reported in Ref. 6; concerning this point, we must remark that the HOPG $s=0.23$ screening value adopted in the above paper has to be considered as a reference value and the consequently obtained sp^2-site percentages have to be seen as maximum values.

TABLE II. Screening factors and sp^2 percentages of the samples.

Sample, x_H (%)	s	sp^2 (%)
0	0.27	59.8
15	0.25	47.3
40	0.32	10.2

The comparison between the optically derived dielectric functions of the samples concerned and those derived from EELS is shown in Fig. 7; as is clear, the two kinds of curve agree in the overall intensity distribution even if the optical result is obviously more resolved than the electronic one. In our opinion this confirms definitively that the REELS technique is a powerful tool to get satisfactory information about the dielectric behavior of a material. It allows also a modeling of the surface scattering response, which could be tentatively related to the joint density of states and electron configuration computed for the surface layers. We must, however, observe the internal difficulties which are encountered in treating the

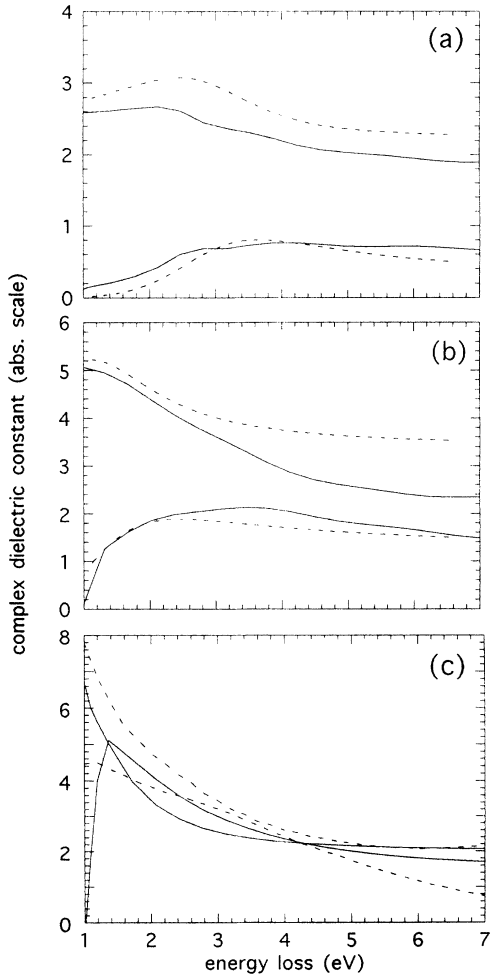

FIG. 7. Comparison of the REELS-deduced (solid lines) and optically deduced (dashed lines) dielectric functions of the materials concerned; (a) α-C:H, $x_H=40\%$; (b) α-C:H, $x_H=15\%$; (c) α-C.

very-low-energy-loss region of the spectra, where effects of experimental origin tend to complicate the analysis and to reduce the confidence in the results when compared with the rest of the spectrum.

In conclusion, the REEL spectra presented immediately lead to three main results: first, from the analysis of the ϵ_2 curves deduced it turns out to be possible to get at least qualitative information on the change in the valence-electronic level distribution when moving from one material to another; in particular, this allows us to make some conclusions about the bonding rearrangement, in terms of sp^2-to-sp^3 ratio, which follows the structural changes in such materials. A comparison of the above-mentioned ratios for the three samples allows us to conclude that sp^2 clustering happens more and more effectively on decreasing the hydrogen content: this fact is reflected in a measurable increase in the π conductivity, which, however, remains less than that of pure HOPG. Even the screening properties appear to change with the average carbon electronic configuration, i.e., with the hydrogen fraction, in the sense that σ electrons screen the π collective excitations more effectively in the less hydrogenated samples. Summarizing all these observation, all the above properties (trigonal percentage, screening factor, conductivity) seem to follow a general trend which would converge finally in the conductive HOPG. Second, the surface single-scattering cross section has been isolated from the bulk one, and this can surely give information on the way in which the optical response of the samples changes when moving towards the surface, at least inside the limits and advantages of the model chosen to describe the dielectric behavior of the surface layers. Third, the complex dielectric functions are obtained in a large energy-loss range with a resolving power that, even not being that of an optical spectroscopic approach, is still good enough to recognize the main single-particle valence-band excitations, as well as the energy location of the plasmonic structures. The quality of our results stands in clear agreement with the optically derived dielectric functions, of course when restricted to the low-energy-loss range which can be probed with a conventional spectrophotometric technique.

[1]D. S. Withmell and R. Williamson, Thin Solid Films **35**, 255 (1976).
[2]L. Holland and S. M. Ojha, Thin Solid Films **38**, L17 (1976).
[3]L. Holland and S. M. Ojha, Thin Solid Films **40**, L31 (1977).
[4]J. J. Cuomo, J. P. Doyle, J. Brulen, and J. C. Lin, Appl. Phys. Lett. **58**, 466 (1991).
[5]A. Bubenzer, P. Dischler, G. Board, and P. Koidl, J. Appl. Phys. **54**, 4519 (1983).
[6]G. Compagnini, L. Calcagno, and G. Foti, Phys. Rev. Lett. **69**, 454 (1992).
[7]J. Robertson and E. P. O'Reilly, Phys. Rev. B **35**, 2946 (1987).
[8]G. Galli, R. M. Martin, R. Car, and M. Parrinello, Phys. Rev. Lett. **62**, 555 (1989).
[9]D. Dasgupta, F. Demichelis, C. F. Pirri, and A. Tagliaferro, Phys. Rev. B **43**, 2131 (1991).
[10]J. Fink, T. Müller-Heinzerling, J. Pflüger, A. Bubenzer, P. Koidl, and G. Crecelius, Solid State Commun. **47**, 687 (1983).
[11]J. Fink, T. Müller-Heinzerling, J. Pflüger, B. Scheerer, B. Dischler, P. Koidl, A. Bubenzer, and R. E. Sah, Phys. Rev. B **30**, 4713 (1984).
[12]A. Terrasi, G. Foti, Y. Hwo, and G. Margaritondo, J. Appl. Phys. **70**, 1885 (1991).
[13]B. L. Doyle and P. S. Peercy, Appl. Phys. Lett. **34**, 811 (1979).
[14]L. Calcagno and G. Foti, Nucl. Instrum. Methods Phys. Res. B **19/20**, 895 (1987).
[15]A. R. Forouhi and I. Bloomer, Phys. Rev. B **34**, 7018 (1986).
[16]G. Compagnini, G. Foti, R. Reitano, and G. Mondio, J. Non-Cryst. Solids (to be published).
[17]W. H. Weber and M. B. Webb, Phys. Rev. **177**, 1103 (1969).
[18]E. T. Arakawa, M. W. Williams, J. C. Ashley, and L. R. Painter, J. Appl. Phys. **52**, 3579 (1981).
[19]G. Mondio, F. Neri, G. Curro', S. Patan, and G. Compagnini, J. Mater. Res. (to be published).
[20]S. Tougaard and J. Kraaer, Phys. Rev. B **43**, 1651 (1991).
[21]E. A. Taft and H. R. Philipp, Phys. Rev. **138**, A197 (1965).
[22]C. Gao, Y. Y. Wang, A. L. Ritter, and J. R. Dennison, Phys. Rev. Lett. **62**, 945 (1989).
[23]S. D. Berger, D. R. McKenzie, and P. J. Martin, Philos. Mag. Lett. **57**, 285 (1988).
[24]N. Savvides, J. Appl. Phys. **59**, 123 (1989).
[25]Y. Wang, H. Chen, R. Hoffman, and J. C. Angus, J. Mater. Res. **5**, 2378 (1990).